INTERNATIONAL JOURNAL OF AUTOMOTIVE AND MECHANICAL ENGINEERING
ISSN: 2229-8649 e-ISSN: 2180-1606
VOLUME 22, ISSUE 2, 2025, 12281 - 12292
DOI: https://doi.org/10.15282/ijame.22.2.2025.3.0940

RESEARCH ARTICLE

Modeling of Creep Behaviour in Grade 91 Steel under Complex State of Stress

I. U. Ferdous[1], N. A. Alang[1,2]*, J. Alias[1,2], A. H. Ahmad[1]

[1]Faculty of Mechanical and Automotive Engineering Technology, Universiti Malaysia Pahang Al-Sultan Abdullah, 26600, Pekan, Pahang, Malaysia
[2]Center for Advanced Industrial Technology (AIT), Universiti Malaysia Pahang Al-Sultan Abdullah, 26600, Pekan, Pahang, Malaysia

ABSTRACT – Power plant components such as boiler tubes, superheated pipes, and headers often operate under elevated temperatures, leading to creep failure. Due to their non-uniform geometries, these components experience complex states of stress. This study investigates the creep rupture characteristics of Grade 91 steel under multiaxial stress conditions, focusing on notched specimens with acuity ratios of 2.28 and 4.56. Creep rupture tests operated at 600°C revealed rupture lives ranging from 52 to 398 hours for the 2.28 acuity ratio and 81 to 890 hours for the 4.56 acuity ratio. Finite element analysis (FEA) incorporating a ductility exhaustion-based damage model predicted rupture lives within a ±2 scatter band of experimental results, demonstrating good agreement. The analysis also highlights those blunter notches show a shift in the locality of extreme damage from the notch root to the ligament center as creep progresses, while sharper notches exhibit localized damage near the notch root. Furthermore, the study establishes the transition between von Mises stress and maximum principal stress-controlled rupture mechanisms. The incorporation of skeletal stress into the Norton power law improved the accuracy of life predictions for non-uniform stress distributions.

ARTICLE HISTORY

Received	:	16th Oct. 2024
Revised	:	28th Jan. 2025
Accepted	:	04th Mar. 2025
Published	:	01st June 2025

KEYWORDS
Creep damage
Grade 91
Norton power law
Notch acuity
Rupture life

1. INTRODUCTION

The creep testing helps to understand material behavior when subjected to continuous load at elevated temperatures. Testing notched specimens becomes essential for components under complex stress states such as those used in coal-fired power plants because it creates multiaxial stress conditions. Grade 91 Steel shows the potential to fulfill the required specifications among existing high Cr steels. It has gained widespread adoption in pressure vessel and pipe systems of fossil power plants and petrochemical facilities because it provides better creep strength and superior thermo-physical properties than 2.25Cr-1Mo steel [1]. The material demonstrates excellent resistance to demanding operational environments, which makes it suitable for critical components in coal-fired power plants that need to maintain high pressure and temperature for maximum efficiency [2]. The 1970s development of Grade 91 steel at Oak Ridge National Laboratory established a major breakthrough in power generation materials through improved performance beyond traditional alloys [3]. The combination of tempered martensite with stable precipitates in its microstructure enables Grade 91 steel to achieve better creep strength and stress corrosion cracking resistance [4]. The power generation industry must understand how Grade 91 steel behaves under long-term loading conditions because this information can guarantee reliable and safe power plant operations.

Conventional creep testing presents major obstacles because of the long experimental durations and substantial financial investments required. Creep tests that replicate real operating conditions can extend up to 100,000 hours, which translates to roughly 12 years, making it impractical for quick material assessment and component design processes. The prolonged evaluation period causes both development delays for new materials and challenges in determining the service life of existing components. The difficulty of reproducing both high temperatures and complex stress states found in power plant components within laboratory environments adds complexity to testing procedures. Researchers now rely on finite element analysis (FEA) and empirical modeling to overcome the testing challenges. These approaches can shorten testing duration while revealing how materials respond to complex stress conditions during creep. Finite element analysis (FEA) provides researchers with a platform to simulate different geometrical configurations and loading conditions, which helps them analyze stress distributions and track damage development in virtual environments [5], [6]. Empirical models built from minimal experimental data enable material behavior predictions across extended time scales, which help estimate long-term creep performance. Notched specimens now direct creep research because they create multiaxial stress states that match the stress conditions found in actual power plant components [7]. Combining notched specimens with FEA and empirical modeling enables researchers to explore creep behavior under realistic conditions while reducing both time and financial expenses associated with conventional testing methods.

Research into the creep behavior of notched specimens continues to attract attention because of its critical implications for component performance under actual operating conditions. Early work by Hayhurst et al. [8] proved that multiaxial stress states play a critical role in predicting creep life by demonstrating how notches significantly change both creep deformation and rupture behavior. Researchers like Webster et al. [9] studied how notch sharpness affects stress

***CORRESPONDING AUTHOR | N. A. Alang** | azuan@umpsa.edu.my

redistribution patterns and damage build-up. Research indicates that notches produce either strengthening or weakening outcomes based on material properties and test conditions. The triaxiality factor, which quantifies notch-induced constraint, significantly affects both creep ductility and damage evolution. Findings by Goyal and Laha [10] demonstrated that Grade 91 steel exhibits extended creep lifespans when circular notches are present instead of smooth surfaces, irrespective of ductility properties, which underscores the intricate relationship between notch shape and material performance. Furthermore, investigations by Wen et al. [11] demonstrated a distinct ductility trough in Grade 91 steel under intermediate stress levels, which indicates the necessity for extensive testing across different conditions to understand material behavior fully.

Finite element analysis serves as an indispensable instrument to simulate creep behavior in notched specimens by delivering insights difficult to achieve through experimental methods alone. Many researchers have utilized FEA to study significant aspects like stress redistribution and damage build-up along with rupture life prediction in notched bars under creep conditions, according to studies [12], [13]. These studies show that accurate constitutive models and damage criteria are essential to represent the complex stress states and failure mechanisms seen in notched geometries accurately [14]. For example, Xu et al. [15] used FEA to show its success in forecasting stress relaxation and redistribution patterns in P91 steel notched specimens and provided essential insights into stress state evolution during creep. Similarly, Zhao et al. [16] used FEA alongside a ductility exhaustion-based damage model to determine creep life estimations for Grade 92 steel with different notch acuities, which demonstrated strong agreement with experimental results. According to Yoshida and Yatomi [17], strain-based damage models yield overly cautious life predictions for notched specimens, which emphasizes the necessity of careful model selection and validation. Researchers have used advanced FEA methodologies with crystal plasticity models to study micromechanical creep deformation features in notched specimens discovering new information about grain-level deformation and its effect on creep behavior.

The Norton power law stands as the primary empirical formulation used to model steady-state creep behavior and determine rupture life. The Norton power law remains essential in creep analysis because it represents creep strain rate through a power-law of applied stress and stands out for its easy-to-use nature and wide-ranging applications [18]. However, researchers have found that single power-law relationships cannot fully describe all aspects of creep behavior since they struggle to represent shifts between short-term and long-term creep processes. For that reason, researchers have introduced bi-linear power-law relations in several studies to address these limitations. [19]. The accuracy of creep predictions across diverse loading conditions improves significantly through the use of separate creep exponents for high- and low-stress regimes in these models. The development of representative stress represents an essential advancement in creep analysis by helping to manage the complex multiaxial stress states present in notched specimens. By combining the contributions of maximum principal stress and von Mises equivalent stress, this approach offers a more precise representation of the driving forces behind creep deformation and damage accumulation [20]. Alang and Nikbin [21] investigated the application of representative stress in creep life prediction, confirming its effectiveness in modeling the complex stress states found in notched geometries. Additionally, Webster et al. [22] proposed the skeletal point method as an alternative technique for characterizing stress states in notched specimens, introducing a way to define representative stresses that remain largely independent of creep properties.

Expanding on earlier studies, this research aims to predict the creep rupture behavior of Grade 91 steel under complex stress conditions by conducting experiments on notched specimens with varying acuity ratios. Furthermore, finite element simulations and empirical modeling using Norton's power law are employed to improve predictions. The study also investigates the transition between von Mises and maximum principal stress-controlled rupture mechanisms, along with the applicability of skeletal stress in life prediction.

2. METHODS AND MATERIALS

2.1 Creep Rupture Test

Test specimens were extracted longitudinally from Grade 91 steel pipe to conduct creep experiments. Eight circumferential notched bar specimens were used to study the effects of constraints and stress states on creep ductility and rupture behavior. The specimens were divided equally, with four having acuity ratios (d/R) of 2.28 and four with ratios of 4.56. The selected acuity ratios (2.28 and 4.56) represent different levels of stress concentration, with the lower value simulating a blunter notch and the higher value representing a sharper notch. These values align with previous studies investigating the role of notch geometry in creep behavior. Figure 1 provides detailed dimensions of these test specimens. With the intention of improving the reliability of the results, additional data were incorporated from literature sources [23]. It's important to note that this supplementary data was derived from ex-service pipes, potentially introducing some creep strength deterioration due to aging effects.

The creep rupture tests were conducted following the procedure outlined in ASTM E292 standard [24]. The net section stresses ranged from 187 MPa to 244 MPa. Specifically, the blunt notch (2.28) and medium notch (4.56) specimens were tested at 210, 220, 230, and 240 MPa, while the literature-sourced double notch (3.0) data included tests at 187, 202, 222, and 244 MPa. The creep tests were conducted using a dead-load creep testing machine equipped with a 1:50 lever ratio for load amplification. Specimens were securely mounted inside the furnace using high-temperature grips, while three K-type thermocouples—positioned at the upper, middle, and lower sections—ensured precise temperature monitoring.

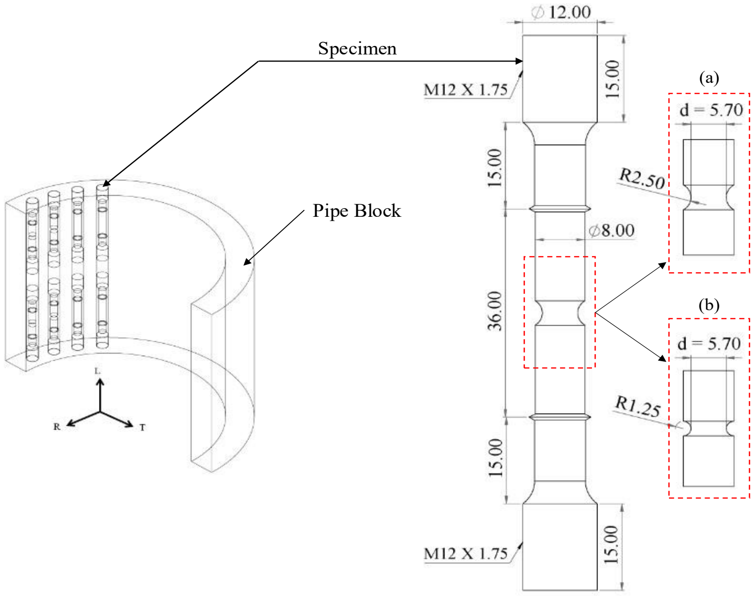

Figure 1. Specified dimension of test specimens: (a) Acuity = 2.28 and (b) Acuity = 4.56

Tests were carried out at a constant temperature of 600°C, with fluctuations rigorously controlled to within ±2°C. A pre-calibrated linear variable differential transformer (LVDT) was attached to the specimen via a clamp-based mounting system to measure axial deformation. Load application was achieved through the lever mechanism, maintaining the target stress throughout the experiment. Displacement data acquisition was performed at 2-minute intervals during primary creep and reduced to 10-minute intervals upon reaching the secondary creep regime. Figure 2 depicts the creep testing machine.

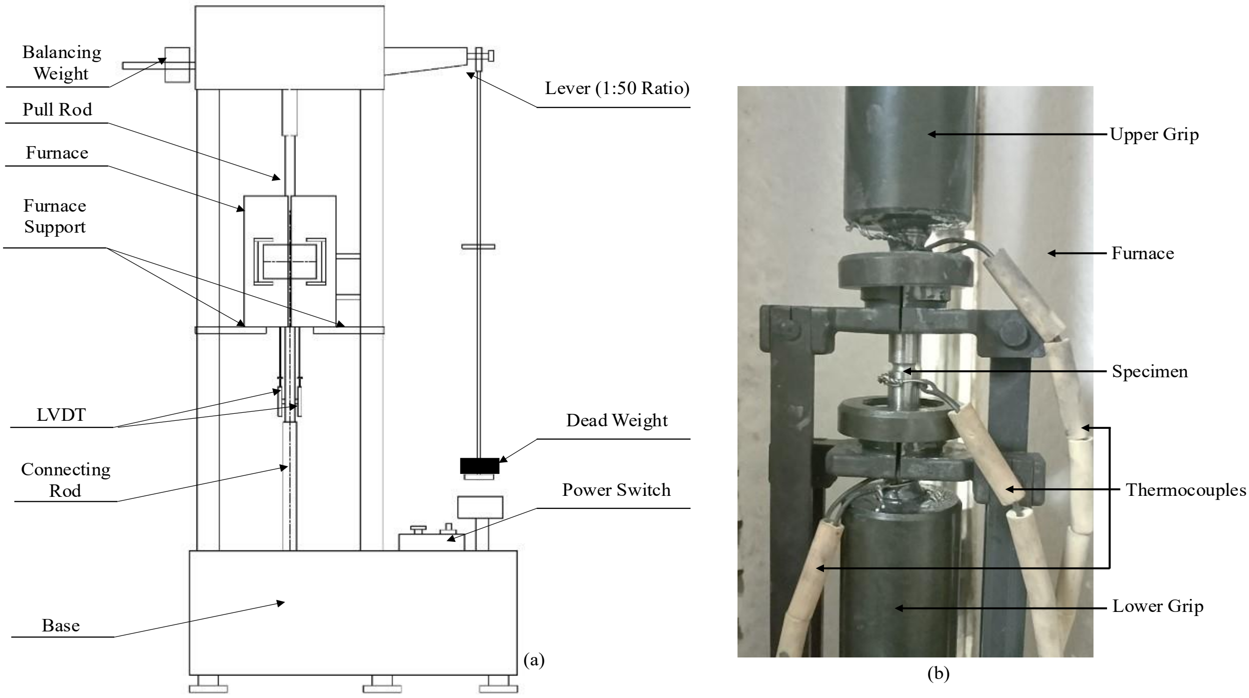

Figure 2. Experimental setup: (a) overall and (b) close-up on creep specimen

2.2 Rupture Life Prediction Using Finite Element Analysis

FE modeling software, ABAQUS v6.14, was employed to conduct finite element analysis using elastic-plastic-creep material properties. Plasticity was modeled using an elastic-plastic-creep approach, where the material's strain-hardening behavior was defined by experimental tensile data. The model accounts for both isotropic hardening and nonlinear stress-strain response before creep initiation. Taking advantage of the specimen's symmetry, one-quarter of each notched bar was modeled using a 2-D axis-symmetric approach. Abaqus partition feature was utilized to create a finer mesh around the notch area, with the smallest element size set to 0.02 mm to ensure accuracy in capturing stress gradients and avoid numerical instability. Meshing was accomplished using quadrilateral elements with a reduced integration scheme (CAX4R). The three FE models contained between 1360-4080 elements and 1479-4245 nodes. The FE mesh was refined sufficiently to accurately capture the total stress distribution and avoid convergence issues during analysis, particularly in the notch root area. Boundary conditions included an applied load on the top surface and y-direction restriction at the bottom surface. Figure 3 provides detailed information about the FE modeling approach.

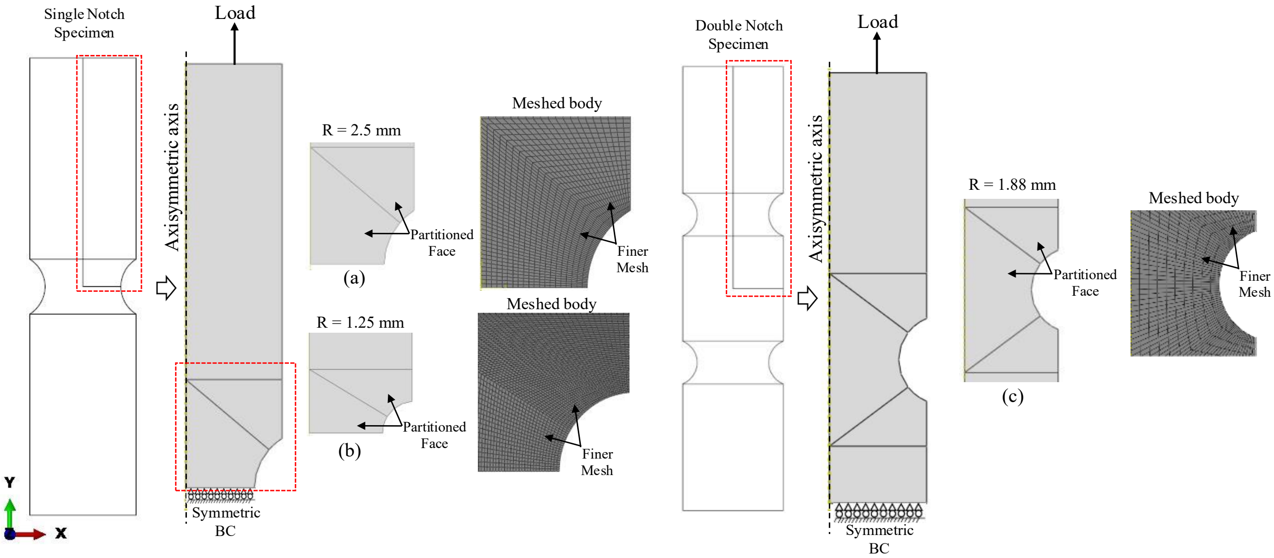

Figure 3. Details FE model with mesh: (a) acuity = 2.28, (b) acuity = 4.56 and (c) acuity = 3.0 (Double Notch)

In the FEA, an elastic-plastic-creep material model was employed. The total strain of the material under creep conditions is represented as the sum of elastic, plastic, and creep components:

$$\varepsilon_T = \varepsilon_e + \varepsilon_p + \varepsilon_c \tag{1}$$

Hooke's law governs elastic strain, while a power law relationship describes plastic strain. For Grade 91 steel at 873 K, the elastic-plastic mechanical properties include an elastic modulus (E) of 164 GPa, strength coefficient (K) of 673.9 MPa, and strain hardening exponent (N) of 0.16 [25]. To establish creep constants A and n, about 69 NIMS [26] creep data points at 600°C has been analyzed. The data conforms to the Norton power-law relation:

$$\dot{\varepsilon}_c = A\sigma^n \tag{2}$$

To improve the accuracy of finite element simulations, distinct creep constants were derived for both short-term (S) and long-term (L) stress regimes. The creep coefficient (A) was numerically modeled using mean, upper-bound, and lower-bound creep curves to account for material variability. The stress exponent (n) remained fixed across analyses to maintain consistency with the minimum creep strain rate slope. Table 1 summarizes the experimentally determined creep properties of Grade 91 steel at 873 K, including characteristic values for both stress regimes.

Table 1. Creep properties of Grade 91 steel at 873 K

Best Fit Curve	$\boldsymbol{A_S}$ (MPa^{-n}/h)	$\boldsymbol{A_L}$ (MPa^{-n}/h)	Stress Exponent, n	
			High Stress, n_S	Low Stress, n_L
Mean	3.77×10^{-35}	1.32×10^{-18}	13.76	5.84
Lower Bound	1.37×10^{-35}	7.32×10^{-19}		
Upper Bound	1.37×10^{-34}	2.32×10^{-18}		

*S signifies as short-term, and L signifies as long-term

The relationship between multiaxial creep ductility, uniaxial creep ductility, and stress triaxiality can be characterized by models such as Cocks and Ashby [27]:

$$\frac{\varepsilon_f^*}{\varepsilon_f} = \sinh\left[\frac{2}{3}\left(\frac{n-0.5}{n+0.5}\right)\right] / \sinh\left[2\left(\frac{n-0.5}{n+0.5}\right)\frac{\sigma_m}{\sigma_e}\right] \tag{3}$$

Uniaxial failure strain varies with strain rate and stress, decreasing with creep time. This suggests distinct controlled failure processes in short and long-term creep. A single mathematical relationship between failure strain and creep strain rate was found to adequately represent the failure strain data for both short-term and long-term stress regimes:

$$\varepsilon_f = \mathrm{f}\,(\dot{\varepsilon}_c) = \frac{\varepsilon_{fmax} + \varepsilon_{fmin}\left(\frac{\dot{\varepsilon}_c}{\dot{\varepsilon}}\right)^{-\alpha}}{\left(\frac{\dot{\varepsilon}_c}{\dot{\varepsilon}}\right)^{-\alpha} + 1} \tag{4}$$

A ductility exhaustion-based damage model was utilized to predict creep life. Failure is anticipated when accumulated creep strain approaches the critical strain:

$$\omega = \int_0^t \dot{\omega} dt = \int_0^t \frac{\dot{\varepsilon}_c}{\varepsilon_f^*} dt \tag{5}$$

The creep damage calculation process involves several steps. First, the creep strain rate is calculated using the Norton power law. Then, the multiaxial creep ductility is determined using the Cocks and Ashby model, which accounts for stress triaxiality. The damage rate is computed as the ratio of creep strain rate to multiaxial creep ductility. This damage rate is integrated over time to obtain the cumulative damage. Local failure is predicted when an element's damage reaches 0.99, at which point its elastic modulus is reduced by 99%. This process is implemented in ABAQUS using a user-defined field subroutine (USDFLD).

2.3 Rupture Life Prediction Using Norton Power Law

In creep regimes, the relationship between creep rupture life and applied stress can be described using a bi-linear power law, as expressed in Eq. (6):

$$t_r = M\sigma^{-\upsilon} \tag{6}$$

This relationship is typically represented on a double-logarithmic scale, with rupture life plotted against applied stress.

Analysis of the Grade 91 steel NIMS data [26] reveals distinct behavior in short-term and long-term stress conditions. For short-term stress, the υ value is approximately 11.36, while for long-term stress, it decreases to about 4.14. This difference, as shown in Table 2, highlights the material's varying response to stress over time.

Table 2. Material parameters of Grade 91 steel

Material Parameters	M	υ
Short term	5.74×10^{27}	11.36
Long term	4.99×10^{12}	4.14

Predicting creep behavior under multiaxial conditions presents unique challenges that uniaxial data alone cannot address. The complex interplay of stress states in multiaxial scenarios affects both creep deformation and rupture in ways not captured by standard uniaxial tests. While Eq. (6) effectively describes uniaxial creep rupture time, adapting it for multiaxial conditions requires the introduction of representative stress. This parameter, incorporating skeletal von Mises and maximum principal stress, replaces the uniaxial stress term in Eq. (6), allowing for a more accurate characterization of multiaxial creep rupture behavior.

$$t_r = M{\sigma_{rep}}^{-\upsilon} \tag{7}$$

The representative stress for multiaxial conditions can be expressed as a combination of skeletal von Mises stress (σ_{VM}^*) and maximum principal stress (σ_1), as shown in Eq. (8) and Eq. (9) for high and low stress conditions, respectively:

$$t_r = M_s[\alpha\sigma_1 + (1-\alpha)\sigma_{VM}^*]^{-\upsilon_s} \qquad \text{High Stress} \tag{8}$$

$$t_r = M_L[\alpha\sigma_1 + (1-\alpha)\sigma_{VM}^*]^{-\upsilon_L} \qquad \text{Low Stress} \tag{9}$$

The application of skeletal stress in these constitutive relations addresses the non-uniform stress distribution characteristic of notched geometries. For practical implementation across varying notch acuities, normalized stress factors - obtained through numerical analysis of notch-region stress fields and scaled by the creep index - provide an effective solution. The code of practice [22] specifies appropriate normalized stress factors for skeletal stress determination. As quantitatively demonstrated in Table 3, the ratios of skeletal von Mises and maximum principal stresses to net section stress are presented for notch acuity ratios of 2.28, 3.0, and 4.56.

Table 3. Normalized stresses for acuity ratio 2.28, 3.0, and 4.56

Acuity ratio	$\frac{\sigma_{VM}^*}{\sigma_{net}}$	$\frac{\sigma_1}{\sigma_{net}}$
2.28	0.80	1.04
3.00	0.77	1.05
4.56	0.73	1.08

The rupture-controlled parameter, α, plays a crucial role in the failure process. This parameter, ranging from 0 to 1, helps estimate rupture life under multiaxial stress. When α equals 1, failure is governed by maximum principal stress; when it's 0, von Mises stress controls failure.

Researchers have developed equations for both scenarios, allowing for the prediction of rupture life under various stress conditions. Equations (10) and (11) represent the case where failure is controlled by von Mises stress (α = 0):

$$t_r = M_s[\sigma_{VM}^*]^{-\upsilon_s} \qquad \text{High Stress} \tag{10}$$

$$t_r = M_L[\sigma_{VM}^*]^{-\upsilon_L} \qquad \text{Low Stress} \tag{11}$$

Conversely, Equations (12) and (13) represent the case where failure is controlled by maximum principal stress (α = 1):

$$t_r = M_s[\sigma_1]^{-\upsilon_s} \qquad \text{High Stress} \tag{12}$$

$$t_r = M_L[\sigma_1]^{-\upsilon_L} \qquad \text{Low Stress} \tag{13}$$

These equations incorporate skeletal von Mises stress (σ_{VM}) and maximum principal stress (σ_1), providing a more comprehensive approach to estimating material behavior under complex stress states.

Figure 4 provides an overview of the prediction techniques used to determine the notched bar's rupture life under creep conditions.

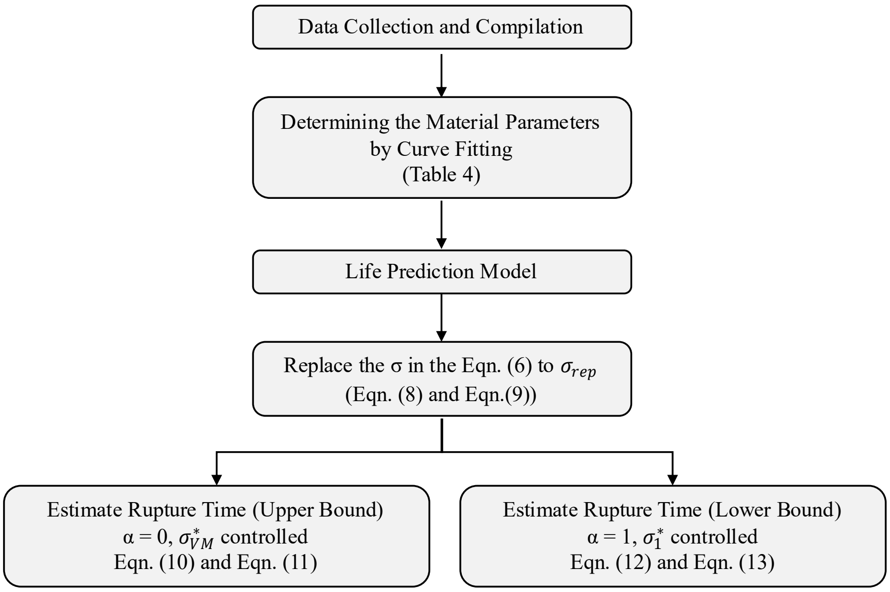

Figure 4. Rupture life prediction using Norton power law incorporating representative stress

3. RESULTS AND DISCUSSION

3.1 Comparison between FE, Empirical and Experimental Rupture Life

A comprehensive finite element analysis was conducted for all acuity ratios (2.28, 3.0, and 4.56) across a range of stress levels. For as-received material (acuity 2.28 and 4.56), the lower bound values of A and n were used, while mean values were applied for ex-service material (acuity 3.0). Figure 5 compares rupture life predictions obtained through Norton Power Law and FE analysis for different notch acuities alongside experimental data. The representative stress replaced uniaxial stress in the Norton power law approach. Two extreme prediction curves were developed using α = 0 (von Mises stress control) and α = 1 (maximum principal stress control) for high and low stress levels, respectively. The transition point between short- and long-term regimes was identified as the intersection of high and low stress expressions. At high stress levels, most experimental data aligned closely with the von Mises stress prediction curve, suggesting plasticity-controlled rupture. As stress decreased, a transition from von Mises to maximum principal stress control was observed. This aligns with the formation of creep cavities in high chromium steel after extended exposure to creep environments, typically at lower stress levels. For acuity 2.28 and 3.0, some data points fell outside the von Mises upper bound curve. This discrepancy may be attributed to the scattered nature of the NIMS creep data used to obtain creep parameters (M and υ), influenced by variations in material batches or heat treatments. Overall, FE predictions showed good agreement with empirical predictions using Norton power law across all acuities. However, this study primarily focused on short-term creep tests, limiting the validation of long-term predictions against experimental data.

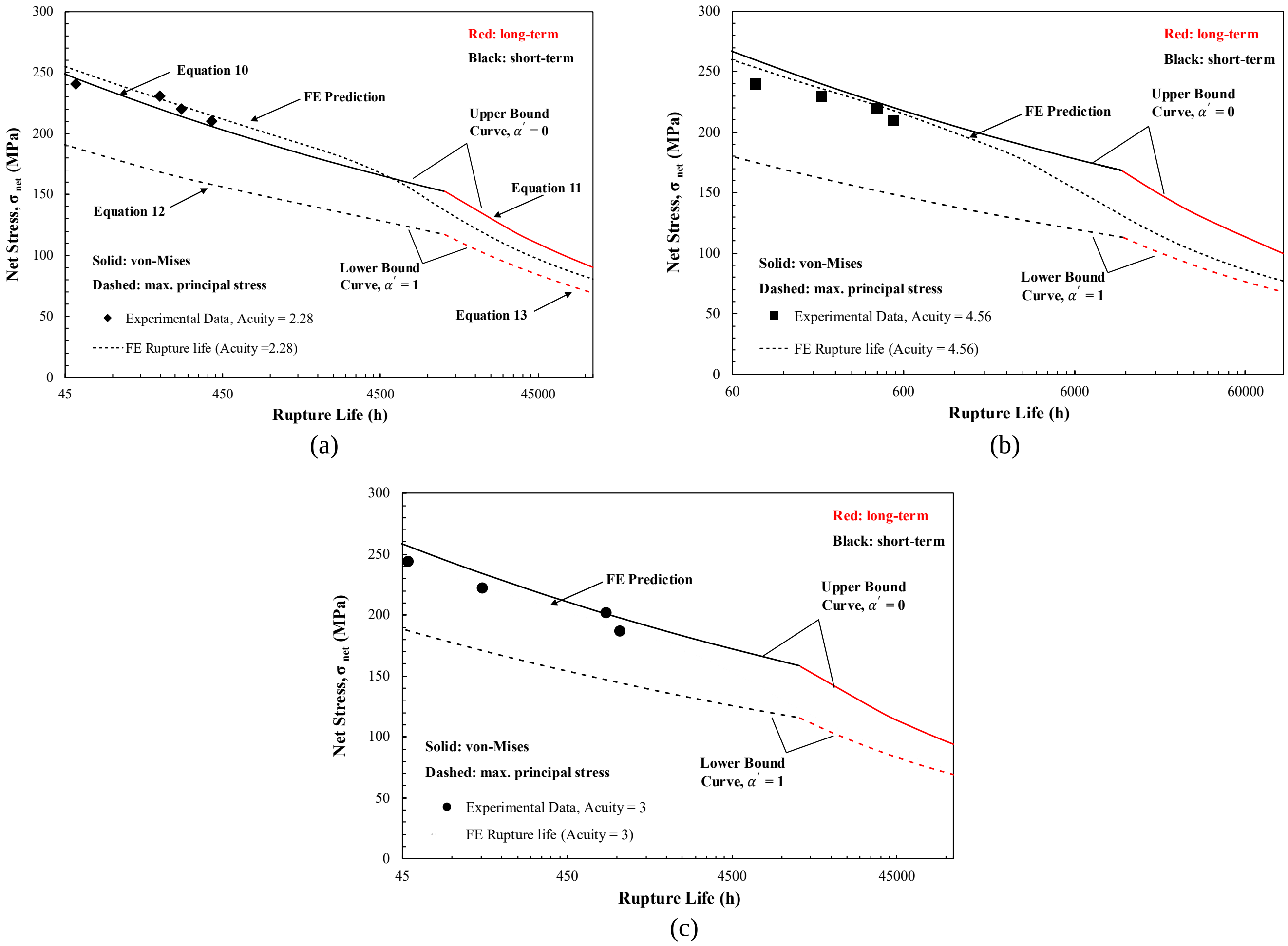

Figure 5. Presents the creep rupture life prediction curves for three distinct notch geometries: (a) acuity ratio 2.28, (b) 4.56, and (c) 3.0

Figure 6 presents an additional evaluation of the model's performance, comparing predicted rupture times against experimental data. This comparison employs a scatter band approach, utilizing a factor of ±2 relative to the experimental values. The graph incorporates two key elements: the predicted vs. experimental data points and the ±2 factor life curves. Notably, all predicted lifetimes fall within this scattered band, indicating good agreement between model predictions and experimental observations. It's crucial to understand the context of this scatter band choice. Creep behavior exhibits high sensitivity to stress levels, with even small changes producing significant effects. A mere 10 MPa shift in stress can often result in a twofold change in creep life. Given this sensitivity, the ±2 factor scatter band provides a practical and conservative approach to assessing prediction accuracy. The application of this particular scatter band is not unique to this study. Similar approaches have been employed in related fields, such as in the analysis of P92 steel creep behavior [16].

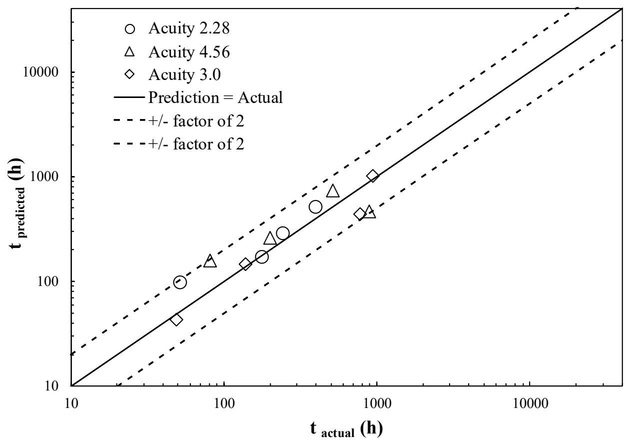

Figure 6. Compares the FE simulated and experimentally observed rupture lives for Grade 91 steel specimens

3.2 Distribution of MPS and von Mises Stress

The analysis of creep damage evolution across different notch acuities revealed consistent patterns in the distribution of Maximum Principal Stress (MPS), von Mises stress and their relationship to damage accumulation. Damage consistently initiated at the notch root and gradually shifted towards the center of the notch as creep progressed, regardless of notch geometry or creep duration. In long-term creep scenarios, typically associated with lower stresses, the MPS distribution closely mirrored the damage pattern, suggesting its dominant role in damage accumulation. Conversely, in short-term creep conditions under higher stresses, the von Mises stress distribution showed a stronger correlation with damage patterns. Notably, the locations of peak stress values consistently aligned with areas of maximum damage. Despite ongoing creep deformation and changes in stress distributions, the site of maximum damage remained relatively stable throughout the creep life of the specimens. While these trends were consistent across all notch acuities, specimens with lower acuity ratios (blunter notches) exhibited a more pronounced shift of the maximum damage zone from the notch root towards the center over time, compared to higher acuity specimens. These observations highlight the complex interplay between stress state, notch geometry, and damage evolution in creep conditions, emphasizing the importance of considering multiple stress measures in comprehensive creep life prediction models.

Analysis of Figure 7 for the acuity level of 2.28 reveals distinct patterns in stress distribution and damage evolution at different stress levels. At lower stress (100 MPa), the maximum principal stress (MPS) and equivalent creep strain intersect slightly away from the notch root. The equivalent creep strain peaks at the notch root, while the MPS reaches its maximum at the ligament's midpoint. Notably, these two parameters converge at a specific location, which likely indicates the point of crack initiation. A similar trend is observed when comparing MPS and damage distribution, with their intersection occurring away from the notch root and their maximum values nearly coinciding. This alignment provides evidence that damage is primarily controlled by MPS at lower stress levels. At higher stress levels (260 MPa), the observed patterns share similarities with the low-stress scenario but with a crucial difference. In this case, the damage appears to be predominantly controlled by von Mises stress rather than MPS. This shift in the controlling mechanism highlights the complex interplay between stress state and damage evolution in notched specimens under varying load conditions.

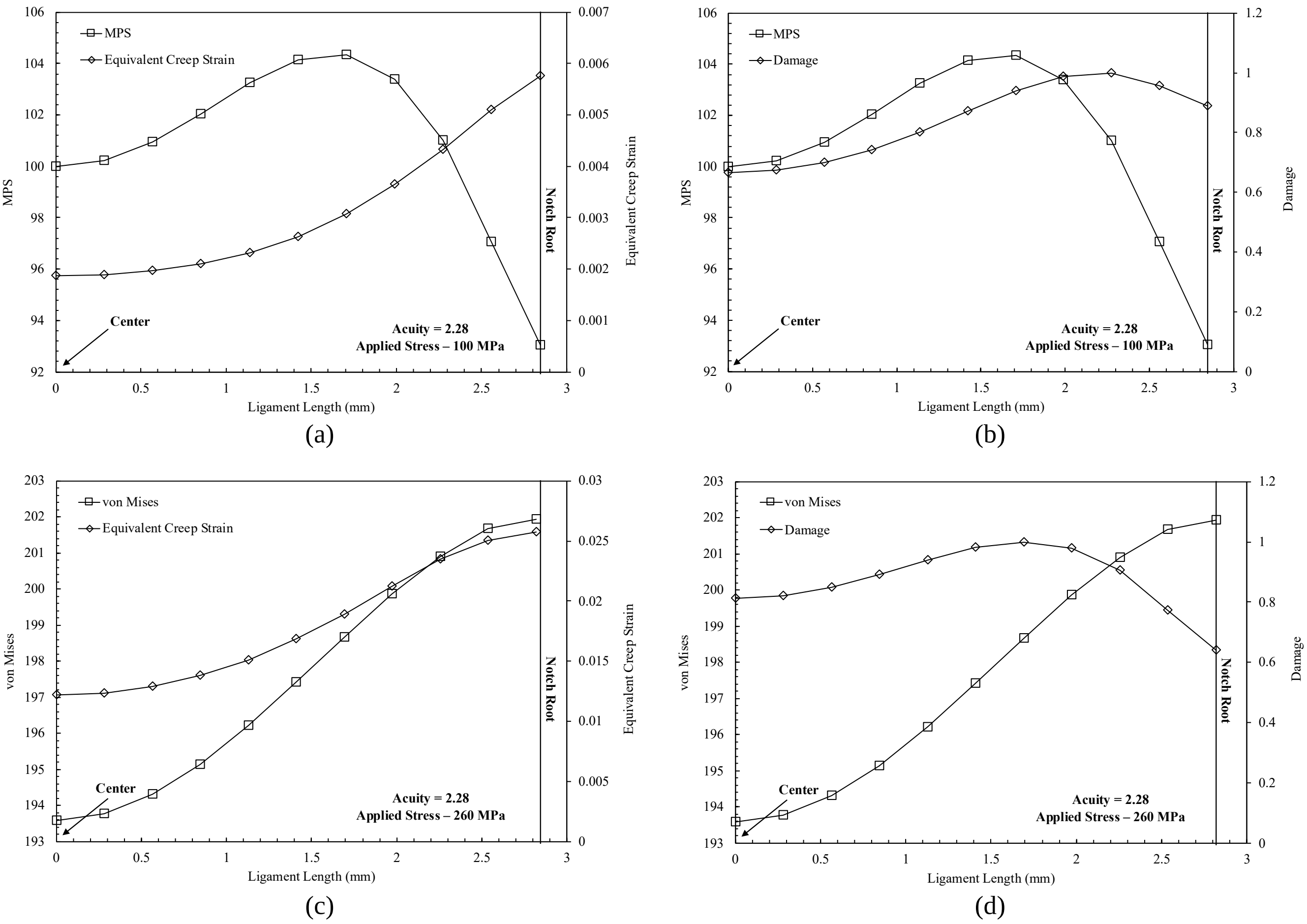

Figure 7. Distribution of maximum principal stress (MPS) and von Mises stress along the ligament length in relation to equivalent creep strain and damage for a notch acuity of 2.28. Results are shown for two stress levels: (a) & (b) 100 MPa, and (c) & (d) 260 MPa

Examination of Figure 8, which depicts results for a notch acuity of 4.56, reveals some distinctions from the 2.28 acuity case. At lower stress (100 MPa), the intersection between MPS and equivalent creep strain occurs closer to the notch root compared to the 2.28 acuity specimen. The maximum values of these parameters are more closely aligned, suggesting a more localized damage initiation zone. The comparison between MPS and damage distribution shows a similar trend, with their peaks nearly overlapping near the notch root. This indicates that for sharper notches, the damage initiation site is more confined to the notch root area, even at lower stress levels. At higher stress (260 MPa), the von Mises stress distribution becomes more prominent in its correlation with damage, similar to the 2.28 acuity case. However, the transition from MPS-controlled to von Mises-controlled damage appears more pronounced in the sharper notch, with a clearer distinction between the two stress regimes. This hypothesizes that this sharper transition may be due to the increased stress concentration factor associated with higher acuity notches.

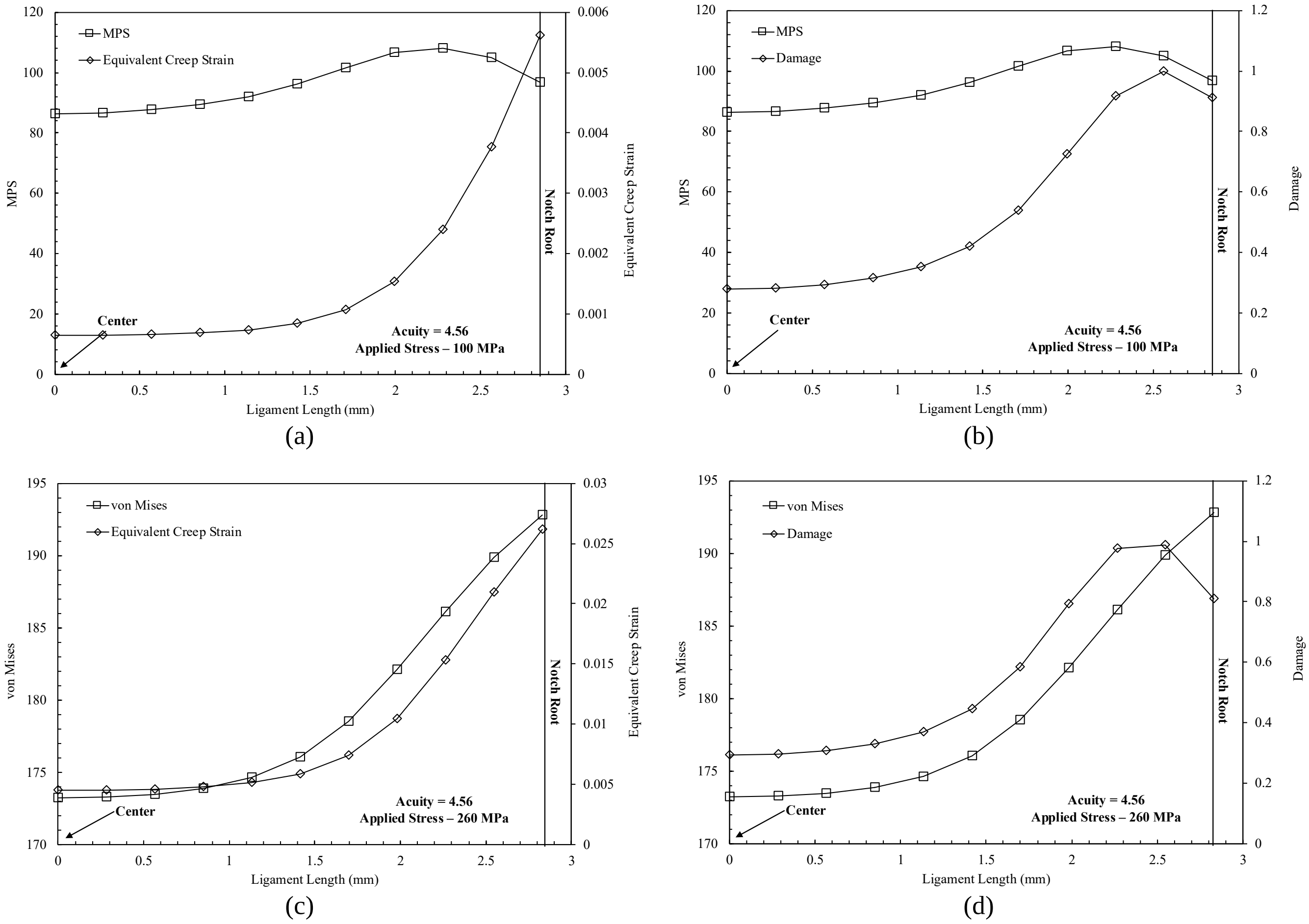

Figure 8: Distribution of maximum principal stress (MPS) and von Mises stress along the ligament length in relation to equivalent creep strain and damage for a notch acuity of 4.56. Results are shown for two stress levels: (a) & (b) 100 MPa, and (c) & (d) 260 MPa

Figure 9, representing the acuity ratio of 3.0, exhibits characteristics that fall between those of the 2.28 and 4.56 acuity specimens. At lower stress (100 MPa), the intersection of MPS and equivalent creep strain occurs at an intermediate distance from the notch root compared to the other two acuities. The damage distribution shows a more gradual transition along the ligament length, suggesting a more distributed damage evolution process. At higher stress (260 MPa), the von Mises stress correlation with damage is evident, but the transition from MPS to von Mises control appears more gradual than in the sharper notch case.

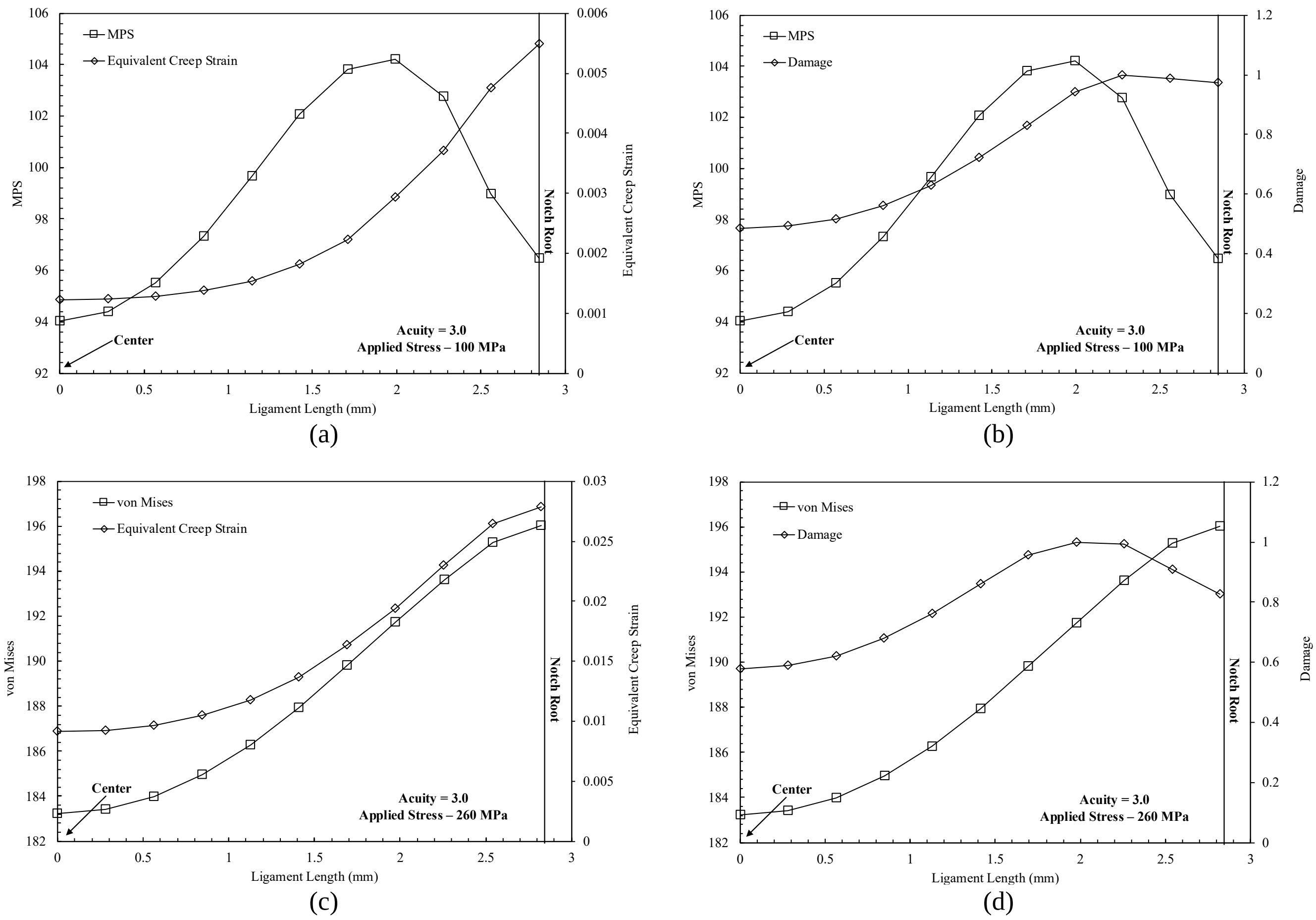

Figure 9: Distribution of maximum principal stress (MPS) and von Mises stress along the ligament length in relation to equivalent creep strain and damage for a notch acuity of 3.0. Results are shown for two stress levels: (a) & (b) 100 MPa, and (c) & (d) 260 MPa

3.3 Evaluation and Distribution of Damage along the Notch Plane

The analysis of creep damage distribution along the notch plane revealed complex patterns that varied with notch acuity and creep progression. For all notch acuities studied (2.28, 3.0, and 4.56), the damage distribution patterns in the notch area remained consistent for identical acuities, regardless of the applied stress levels. This consistency suggests that the notch geometry plays a fundamental role in dictating the damage evolution process.

For specimens with an acuity of 2.28 (blunt notches), the initial stages of creep deformation (approximately 10% of rupture life) were characterized by maximum damage concentration near the notch root. This localization can be attributed to the stress concentration effect induced by the notch geometry. As creep progressed to about 50% of rupture life, a significant redistribution of stress occurred due to variations in creep rates and stress triaxiality across the notch plane. Consequently, the zone of maximum damage began to shift towards the notch center and expanded to encompass a broader area around the notch. By the later stages of creep life (around 90% of rupture life), the escalating damage level prompted a final shift of the maximum damage zone towards the notch center. This shift is believed to occur to maintain strain compatibility, resulting in a cup-and-cone rupture pattern that aligns with experimental observations. Importantly, this phenomenon persisted across all applied loads for the 2.28 acuity notch. In contrast, specimens with a notch acuity of 4.56 (sharp notches) displayed markedly different behavior. The movement of the maximum damage zone was less pronounced throughout the creep process. Damage initiation at early stages (10% of rupture life) and subsequent propagation remained concentrated near the notch root until the late stages of creep life (90% of rupture life). This suggests that for sharp notches, the location of peak damage remains relatively constant throughout the creep process. Furthermore, the spread of damage along the ligament length was limited, with most areas maintaining low damage levels even at 90% of rupture life. This trend was consistent across all applied loads for the 4.56 acuity specimens.

Specimens with a notch acuity of 3.0 exhibited behavior intermediate between the 2.28 and 4.56 acuity specimens. Initially, maximum damage occurred near the notch root, but as creep progressed, there was a noticeable migration of the damage zone towards the notch center, though less pronounced than in the 2.28 acuity specimens. These findings collectively suggest a clear trend: as notch acuity decreases (i.e., as notches become blunter), the location of maximum damage tends to shift more prominently from the notch root to the notch center over time. This behavior can be attributed to the different stress states induced by varying notch geometries and their evolution during creep. An important observation was that blunt notches exhibited creep damage accumulation over a larger portion of the ligament length compared to medium and sharp notches. This broader distribution of damage correlates with the improved creep life observed in medium-notched specimens compared to blunt-notched ones. The more localized damage in sharper notches may lead to earlier crack initiation but slower propagation, while the broader damage distribution in blunter notches may delay crack initiation but lead to faster propagation once a crack forms. It is noteworthy that the time required for complete damage of a few elements near the notch root did not differ significantly from the time needed for damage development across the entire notch ligament. This suggests an absence of stable crack growth prior to rupture, indicating that the failure process in these notched specimens is dominated by distributed damage accumulation rather than discrete crack propagation.

4. CONCLUSIONS

This investigation of the creep behavior of Grade 91 steel under multiaxial stress conditions has yielded several important findings. The combined approach of experimental testing, finite element analysis, and empirical modeling has provided a comprehensive understanding of creep damage evolution and rupture life prediction for notched specimens. The study demonstrated that notch acuity plays a crucial role in determining the location and progression of creep damage, with blunter notches exhibiting a shift in maximum damage location over time. The finite element simulations, incorporating a ductility exhaustion-based damage model, successfully captured the creep damage evolution and rupture life across various notch acuities and stress levels, with predictions falling within a factor of ±2 scatter band of experimental data. The empirical modeling approach, based on the Norton power law and incorporating the concept of representative stress, provided valuable insights into the transition between von Mises and maximum principal stress-controlled rupture mechanisms. The introduction of skeletal stress considerations improved the accuracy of predictions for non-uniform stress distributions in notched specimens. While primarily based on short-term creep tests, this research contributes significantly to the development of more accurate life prediction methodologies for high-temperature power plant components. Future work could focus on extending these findings to a broader range of notch geometries and longer-term creep conditions to further refine predictive capabilities for Grade 91 steel and similar high-temperature alloys.

ACKNOWLEDGEMENTS

The authors gratefully acknowledge the financial support provided by the Ministry of Higher Education (MOHE) Malaysia through the Fundamental Research Grant Scheme FRGS/1/2023/TK10/UMP/02/11 (University Reference: RDU230109) and also would like to express their gratitude to the Universiti Malaysia Pahang Al-Sultan Abdullah (UMPSA) for additional funding under the Postgraduate Research Grant Scheme PGRS230387.

CONFLICT OF INTEREST

The authors declare that there are no conflicts of interest associated with this publication.

AUTHORS CONTRIBUTION

I.U. Ferdous: Conducted the creep tests and finite element analysis, performed data analysis, interpreted the results, contributed to the discussion, and prepared the final manuscript.

N.A. Alang: Conceived and designed the research, conducted creep tests, contributed to the interpretation and discussion of results, secured funding, provided English language editing, and participated in the preparation of the final manuscript.

J. Alias: Contributed to the interpretation of results and critically revised the final manuscript.

A.H. Ahmad: Reviewed and revised the final manuscript for intellectual content.

REFERENCES

[1] I. U. Ferdous, N. A. Alang, J. Alias, A. H. Ahmad, and S. Mohd Nadzir, "Rupture life and failure mechanism of Grade 91 steel under the influence of notch constraint," *Journal of Failure Analysis and Prevention*, vol. 23, no. 2, pp. 497–510, 2023.

[2] H. Shigeyama, Y. Takahashi, J. Siefert, and J. Parker, "Creep-Fatigue life evaluation for Grade 91 steels with various origins and service histories," *Metals (Basel)*, vol. 14, no. 2, p. 148, 2024.

[3] B. A. Prajapati and J. A. Penso, "Fabrication of Grade 91 materials experience in oil and gas applications," in *Pressure Vessels and Piping Conference*, American Society of Mechanical Engineers, p. V006T06A060, 2020.

[4] A. Tonti, A. Alvino, A. Antonini, C. Delle Site, D. Lega, S. Matera, and et al., "Steel grades 91 and 92 microstructure and precipitate evolution atlas and life assessment tool," *Materials at High Temperatures*, vol. 41, no. 2, pp. 222–233, 2024.

[5] N. A. Alang and K. Nikbin, "Creep, fatigue, and creep-fatigue crack growth behaviours of P92 steel at 600 °C," *Strength, Fracture and Complexity*, vol. 15, no. 1, pp. 29–45, 2022.

[6] N. A. Alang and K. Nikbin, "Modelling of creep rupture in Grade 92 steel using a microstructure-type finite element mesh," *Key Engineering Materials*, vol. 946, pp. 29–34, 2023.

[7] N. A. Alang, L. Zhao, and K. Nikbin, “Evaluation of Monkman–Grant strain as a key parameter in ductility exhaustion damage model to predict creep rupture of Grade 92 steel,” *Journal of Strain Analysis for Engineering Design*, vol. 57, no. 5, pp. 392–408, Jun. 2022.

[8] D. R. Hayhurst, F. A. Leckie, and C. J. Morrison, “Creep rupture of notched bars.,” *Proceedings of the Royal Society A*, vol. 360, no. 1701, pp. 243–264, 1978.

[9] G. A. Webster, K. M. Nikbin, and F. Biglari, “Finite element analysis of notched bar skeletal point stresses and dimension changes due to creep,” *Fatigue & Fracture of Engineering Materials & Structures*, vol. 27, no. 4, pp. 297–303, 2004.

[10] S. Goyal, K. Laha, C. R. Das, and M. D. Mathew, “Analysis of creep rupture behavior of Cr-Mo ferritic steels in the presence of notch,” *Metallurgical and Materials Transactions A*, vol. 46, no. 1, pp. 205–217, 2015.

[11] J. F. Wen, S. T. Tu, F. Z. Xuan, X. W. Zhang, and X. L. Gao, “Effects of stress level and stress state on creep ductility: Evaluation of different models,” *Journal of Materials Science & Technology*, vol. 32, no. 8, pp. 695–704, 2016.

[12] N. Bieberdorf, A. Tallman, M. A. Kumar, V. Taupin, R. A. Lebensohn, and L. Capolungo, “A mechanistic model for creep lifetime of ferritic steels: Application to Grade 91,” *International Journal of Plasticity*, vol. 147, p. 103086, 2021.

[13] I. U. Ferdous, N. A. Alang, J. Alias, and S. M. Nadzir, “Numerical prediction of creep rupture life of ex-service and as-received Grade 91 steel at 873 K,” *International Journal of Automotive and Mechanical Engineering*, vol. 18, no. 3, pp. 8845–8858, 2021.

[14] T.-Y. Niu, C. Gong, J.-G. Gong, and F.-Z. Xuan, “Creep failure behavior of notched structure in the simulated steam turbine rotor: Experimental and damage analysis,” *Journal of Pressure Vessel Technology*, vol. 142, no. 6, 2020.

[15] X. Xu, G. Z. Wang, F. Z. Xuan, and S. T. Tu, “Effects of creep ductility and notch constraint on creep fracture behavior in notched bar specimens,” *Materials at High Temperatures*, vol. 33, no. 2, pp. 198–207, 2016.

[16] L. Zhao, N. A. Alang, and K. Nikbin, “Investigating creep rupture and damage behaviour in notched P92 steel specimen using a microscale modelling approach,” *Fatigue & Fracture of Engineering Materials & Structures*, vol. 41, no. 2, pp. 456–472, 2018.

[17] K. Yoshida and M. Yatomi, “Creep damage evaluation for HAZ of Mod. 9Cr-1Mo steels under multiaxial stress conditions,” *Procedia Engineering*, vol. 10, pp. 490–495, 2011.

[18] F. H. Norton, *The creep of steel at high temperatures*, 1st ed. New York: McGraw-Hill Book Co., 1929.

[19] B. K. Choudhary and J. Christopher, “Influence of temperature and strain rate on tensile deformation and fracture behaviour of boron added P91 steel,” *International Journal of Pressure Vessels and Piping*, vol. 171, pp. 153–161, 2019.

[20] H. A. Lockwood, M. H. Agar, and S. M. Fielding, “Power law creep and delayed failure of gels and fibrous materials under stress,” *Soft Matter*, vol. 20, no. 11, pp. 2474–2479, 2024.

[21] N. A. Alang and K. Nikbin, “A new approach to predict creep rupture of Grade 92 steel under multiaxial stress states,” *International Journal of Mechanical Sciences*, vol. 163, p. 105096, 2019.

[22] G. A. Webster, S. R. Holdsworth, M. S. Loveday, K. Nikbin, I. J. Perrin, H. Purper, et al., “A code of practice for conducting notched bar creep tests and for interpreting the data,” *Fatigue & Fracture of Engineering Materials & Structures*, vol. 27, no. 4, pp. 319–342, 2004.

[23] N. A. Razak, “Creep and creep-fatigue Interaction in new and service exposed P91 steel,” Thesis, Imperial College London, 2018.

[24] ASTM International Committee E-28 on Mechanical Testing. *Standard test methods for elevated temperature tension tests of metallic materials*. ASTM International, 2009.

[25] J. J. Han, H. S. Lee, Y. J Kim, N. H. Kim, W. G. Kim, H. Y. Lee, et al., “Prediction of creep crack initiation and growth for P91 at 600°C using MOD-NSW model,” *Strength, Fracture and Complexity*, vol. 9, no. 1, pp. 125–136, 2015.

[26] K. Sawada, K. Kimura, F. Abe, Y. Taniuchi, K. Sekido, T.Nojima, and T.Ohba et al., “Catalog of NIMS creep data sheets,” *Science and Technology of Advanced Materials*, vol. 20, no. 1, pp. 1131–1149, 2019.

[27] A. C. F. Cocks and M. F. Ashby, “On creep fracture by void growth,” *Progress in Materials Science*, vol. 27, no. 3–4, pp. 189–244, 1982.